Analyzing the Dynamic Behavior of a High Aspect Ratio Wing Incorporating a Folding Wingtip

R.C.M. Cheung[1], D. Rezgui[2] and J.E. Cooper[3]
Department of Aerospace Engineering, University of Bristol, University Walk, Bristol, BS8 1TH, UK.

and
T. Wilson[4]
Airbus Operations Ltd, Filton, Bristol, BS34 7PA, UK.

High aspect ratio wings have been the focus of recent aircraft designs for improving fuel efficiency through induced drag reduction. The lengthened wingspan derived from these designs have led to the introduction of folding wingtips in order to meet airport gate width requirements. Previous numerical and experimental studies have demonstrated that folding wingtips can also provide a gust load alleviation benefit, when the folding wingtips are able to rotate freely about the hinge during the gust encounter. This work examines the dynamic characteristics and behavior of the folding wingtip, and the overall wing in such a configuration. A series of wind tunnel tests was conducted using a specially designed high aspect ratio wing model to establish its modal characteristics through application of a stepped-sine frequency sweep, performed using a gust generator as well as a secondary aerodynamic surface incorporated into the wingtip as the excitation source. In addition, a pseudo-random gust sequence was used as a faster test method through broadband excitation, which yielded results that were in excellent agreement with the stepped-sine methods.

Nomenclature

Symbols

α	=	Angle of attack
γ	=	Hinge angle
θ	=	Fold angle of the wingtip
f	=	Frequency
v	=	Wind tunnel velocity

I. Introduction

It is well known that aircraft designs employing higher aspect ratio wings are aerodynamically beneficial due to the reduction of induced drag, leading to better fuel efficiency and reduced environmental effect. However, the increased structural weight from the longer wingspan could offset the gains obtained from the aerodynamics. The lengthened wingspan could also pose operational difficulties as existing airport gates are likely to be too narrow. Consequently, a wingtip folding mechanism is available on the latest B-777 aircraft for use on the ground to overcome this restriction[1].

The advent of folding wingtips in modern airliners has also enabled research into utilizing them as a new type of gust load alleviation device. Sizing of aircraft structures is mostly driven by the critical load cases from gusts and maneuvers, therefore effective loads alleviation can lead to lighter weight, more fuel-efficient and environmentally

[1] Research Associate, Department of Aerospace Engineering.
[2] Lecturer in Aerospace Engineering, Department of Aerospace Engineering.
[3] Airbus Royal Academy of Engineering Sir George White Professor of Aerospace Engineering, FAIAA.
[4] Loads and Aeroelastics, Flight Physics Department.

friendly aircraft. By incorporating an appropriate hinge geometry, a folding wingtip can function as a passive gust load alleviation device. This benefit originates from the geometric relationship between the orientation of the wingtip folding axis and the change in the effective local angle of attack of the wingtip as it folds, which is described by

$$\Delta\alpha_{WT} = -\tan^{-1}(\tan\theta \sin\gamma) \quad (1)$$

where the hinge angle γ denotes the orientation of the folding axis from the longitudinal axis of the aircraft and the fold angle θ refers to the angular displacement of the wingtip from the wing-level position, as shown in Figure 1 and Figure 2 respectively.

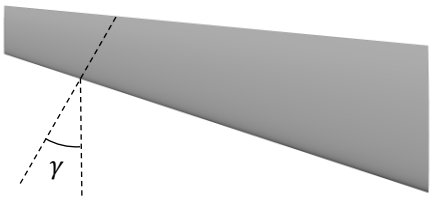

Figure 1 Hinge angle γ.

Figure 2 Fold angle θ.

Figure 3 shows that a zero-valued hinge angle provides no changes to the local angle of attack of the wingtip during folding, leading to no additional gust load alleviation. However, with a positive hinge angle implemented, as seen in Figure 4, the local angle of attack of the wingtip decreases with the folding action, which can reduce its bending moment contribution during a vertical gust encounter and thus achieving gust load alleviation.

Figure 3 0-deg hinge angle.

Figure 4 30-deg hinge angle.

A previous study by the authors[2] investigating non-zero-value hinge angle configurations and variation in the folding hinge stiffness demonstrated that the peak wing root bending moment could be reduced by allowing the wingtip to fold during gust encounters. This finding agrees with several other studies[3-5] that showed that a lower folding hinge stiffness tended to improve the gust load alleviation performance.

By allowing the folding wingtip to rotate freely about the hinge inflight, an additional degree of freedom is introduced to the aeroelastic system of the wing which warrants closer examination to help understand its effect on the dynamic behavior of the overall system. One key observation, already established from previous experimental works[2, 6], is the reduction of peak wing-root bending moment in one-minus-cosine gust conditions. However, very limited test-based dynamic analysis of the folding wingtip concept has been performed.

In this paper the dynamic behavior of a flexible wing with a folding wingtip is investigated in more detail than previously. The experiments used a wind tunnel prototype in a low speed wind tunnel, with excitation provided by a gust generator as well as a secondary aerodynamic surface incorporated into the folding wingtip. A series of sinusoidal excitations were used to obtain modal characteristics in a similar fashion to a conventional stepped-sine sweep. In addition, a pseudo-random gust sequence was used to excite the wind tunnel model, allowing investigation of the response of the folding wingtip and the wing in unsteady atmospheric conditions.

II. Wind Tunnel Model

A. Design

The current work aims primarily to improve the understanding of how the folding wingtip concept may be applied to a flexible high aspect ratio wing for reducing the peaking loading during a gust encounter. For this reason, the current wind tunnel model has a semi-span of 1.345m, with a constant chord length of 0.150m. The equivalent full-wing aspect ratio is 17.9, which is a significant increase from the aspect ratio of 6.7 used in the previous study. The same constant sectional profile of NACA0015 has been retained for consistency and internal clearance for sensors and servo cable routing. Unlike the previous model, the section inboard of the folding hinge is considerably more flexible in out-of-plane bending. Structural stiffness of this section is provided by a 316L stainless steel beam that spans from the wing-root to the folding hinge section, covered by several skin panels for the required aerodynamic profile. As shown in Figure 5(a), these skin panels are intentionally spaced apart to avoid touching even when the magnitude of wing bending is large, such that the overall bending and torsional stiffness of the wing remain similar to that of the underlying beam. The wingtip folding hinge is oriented at a hinge angle of 10.0 deg, and at the mid-chord position along the hinge line, it measures 1.000m spanwise from the wing-root. In this arrangement, the folding wingtip constitutes 26% of the total wetted area of the entire wing.

As shown in Figure 5(a) and (b), a movable secondary aerodynamic surface, referred to as the wingtip tab, is featured on the folding wingtip at the 75% chord position. The wingtip tab has a span of 0.100m and it is driven directly by a Maxon[7] EC-i30 brushless motor for active control.

B. Instrumentation

The wind tunnel model is equipped with an RLS RM08 magnetic encoder[8] at the folding hinge for measuring the fold angle of the wingtip. There is a total of six accelerometers installed in the wind tunnel model, consisting of an Endevco Model 65L[9], a PCB Piezotronics[10] 356A32, a PCB Piezotronics 352C65 and three PCB Piezotronics M352C65. For clarity, the locations of these accelerometers are summarized in Table 1. Four Vishay Micro-measurements[11] CEA-09-125UN strain gages in full-bridge configuration are installed on the main beam to provide wing-root bending moment measurement. The total load on the wind tunnel model was measured using a custom-built balance equipped with an AMTI MC3A-1000[12] and an AMTI MC3A-250 load cell. An iMetrum[13] ICA-3D-1000-03 camera system was used to monitor deflection of the wind tunnel model during the gust excitations. The accelerometers, encoder and strain gages were connected to a National Instruments[14] PXIe-1082 chassis, equipped with PXIe-6363, PXIe-4492 and PXIe-4330. MATLAB[15] was used for data acquisition and generation of wingtip tab deflection demand signal. An iMetrum ICA-3D-1000-03 camera system was also set up to track deflection of the wind tunnel model under load. The main purpose of using this camera system was to correlate accelerometer measurements, since the low end of the frequency test range was near the accelerometers' measurement limit.

Table 1. Accelerometer locations.

Label	Model	Span Location (m)	Chord Position (%)
Wing-inboard	M352C65	0.295	25
Wing-inboard 0.6c	M352C65	0.295	60
Hinge-inboard	356A32	0.820	11
Hinge-inboard 0.6c	M352C65	0.820	60
Wingtip	65L	1.337	12
Wingtip 0.6c	352C65	1.337	60

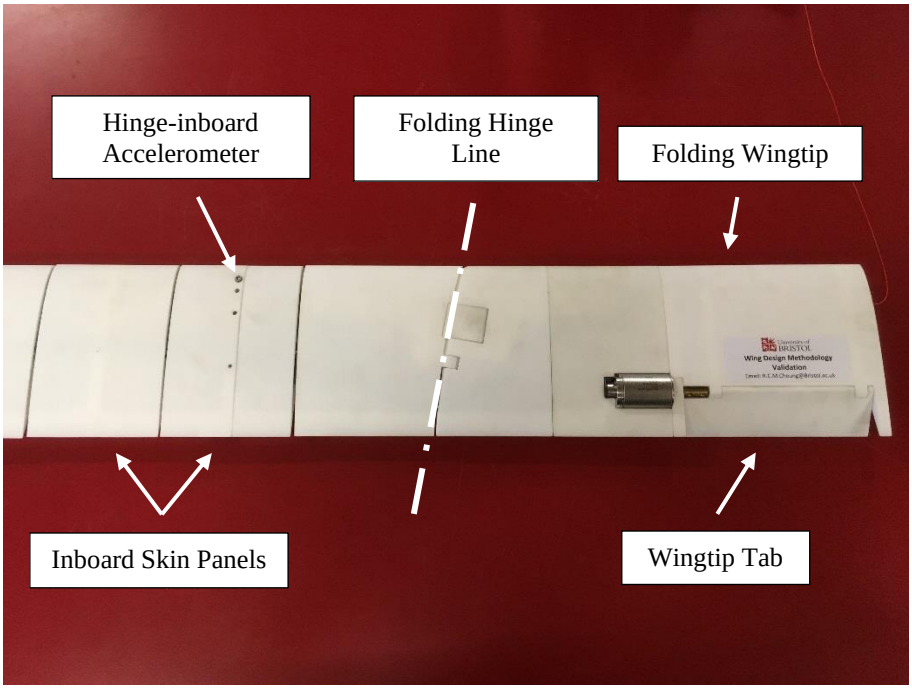

(a) Folding hinge section.

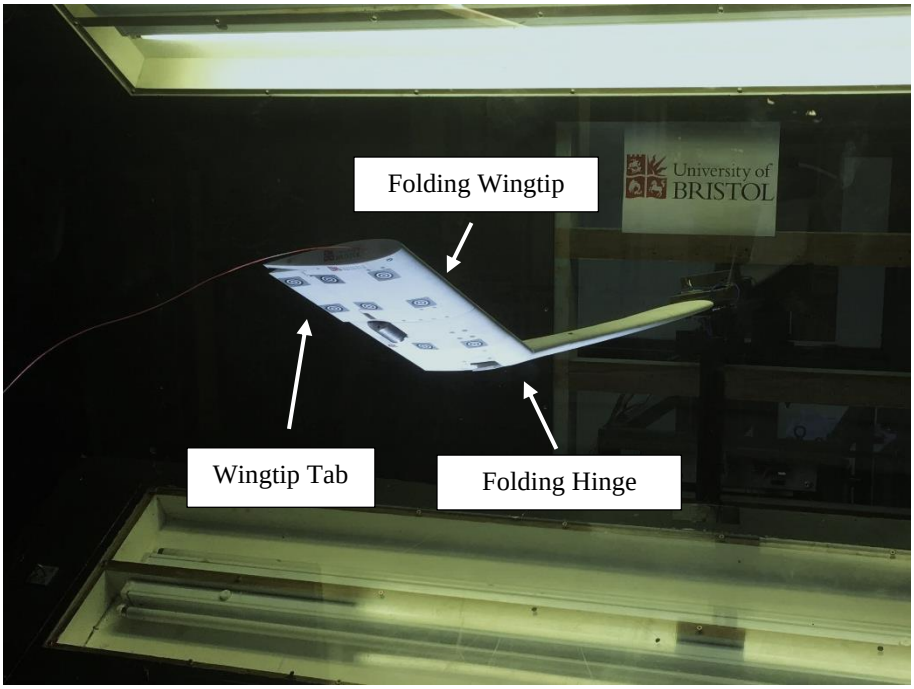

(b) Free-hinge configuration.

Figure 5 Wind tunnel model.

C. Testing

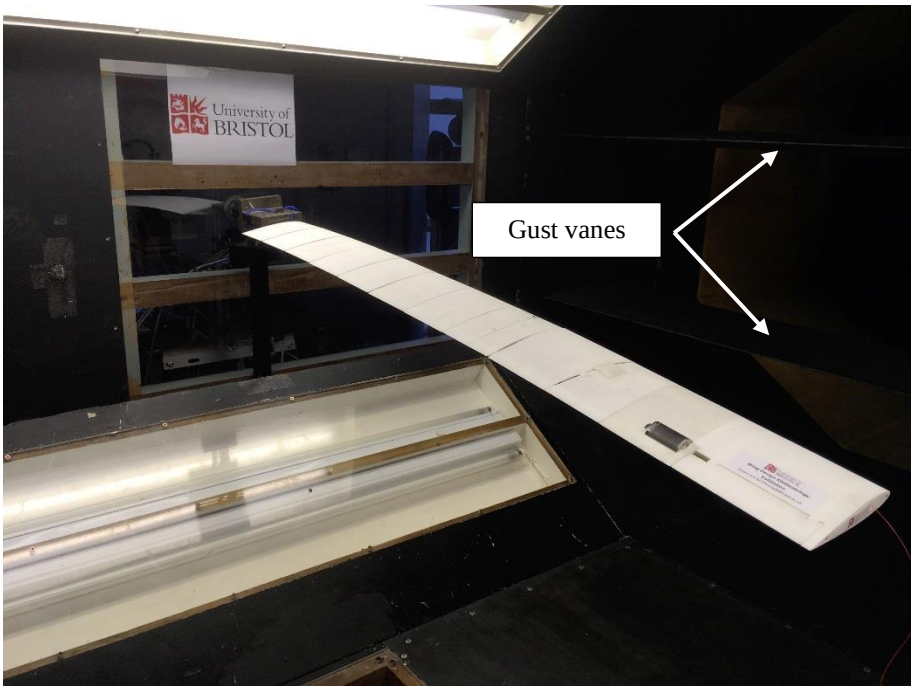

Figure 6 Working section of the 7ft by 5ft wind tunnel at the University of Bristol.

Testing was carried out in the 7ft by 5ft low-speed closed-return wind tunnel at the University of Bristol, which is equipped with a dual-vane vertical gust generator[16] as shown in Figure 6. In the test campaign, the wind tunnel model was first subjected to a series of stepped sinusoidal gust excitations, such that the modal characteristics could be identify in a similar fashion to a conventional frequency sweep through a shaker. A second series of tests used the wingtip tab as the means of frequency excitation instead, with the aim of the experiment remaining the same. The third part of the test involved using a pre-defined pseudo-random gust sequence to provide a broadband frequency excitation, with the goal of enabling modal identification using a shorter test duration.

In each test, the wind tunnel model was nominally set to a configuration in which the wingtip could freely rotate about the folding hinge. When appropriate, a baseline reference was obtained by locking the wingtip in the wing-level orientation. These two configurations of the wingtip are referred to as the free-hinge and the locked-hinge cases.

III. Results

A. Stepped-sine frequency sweep using gust generator

A series of stepped sinusoidal gust excitations up to 10.0Hz was used to establish the frequency response of the wind tunnel model. The test condition was set to an angle of attack of 5.0 degrees and wind tunnel velocity of 18.0m/s, with peak gust vane deflection of 3.0 degrees. For a constant peak gust vane angle, the magnitude of gust output varies with the required actuation frequency and wind tunnel velocity. Therefore, the gust response shown in this work is corrected according the gust generator characteristics shown in Figure A.1 in the appendix.

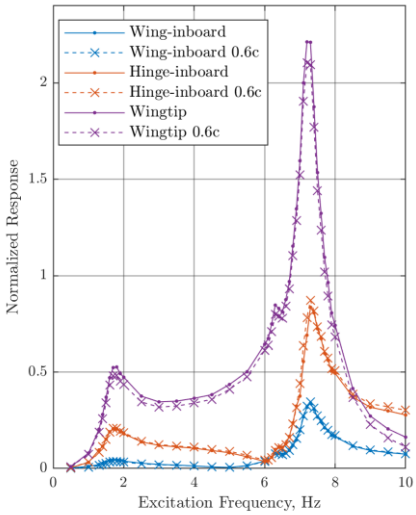

(a) The locked-hinge configuration.

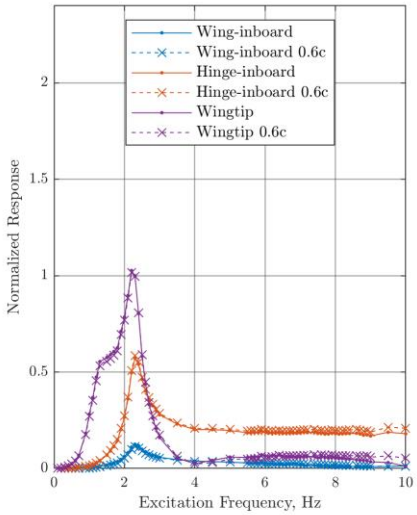

(b) The free-hinge configuration.

Figure 7 Out-of-plane acceleration due to gust excitation.

As shown in Figure 7(a), the first and second out-of-plane bending modal frequency in the locked-hinge configuration are at 1.6Hz and 7.3Hz respectively. For the free-hinge configuration, the first out-of-plane bending modal frequency is 2.3Hz as indicated by Figure 7(b). The increase in the first out-of-plane bending modal frequency is an expected observation, since releasing the folding hinge shortens the equivalent bending length of the wing.

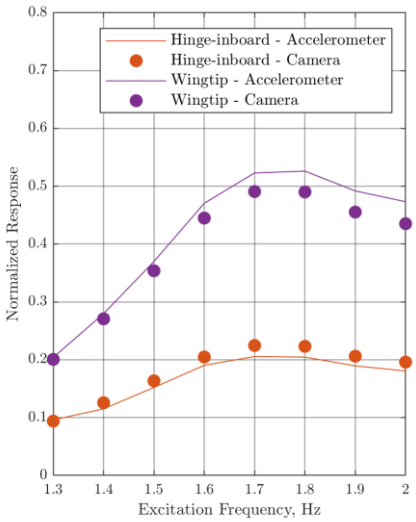

(a) The locked-hinge configuration.

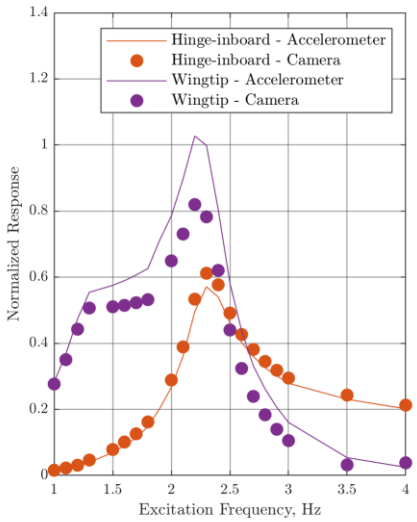

(b) The free-hinge configuration.

Figure 8 Comparison of camera-derived out-of-plane acceleration and accelerometer measurements.

Although the first out-of-plane bending modal frequency in both configurations are near the lower frequency response limit of the IEPE accelerometers used, the measurements collected correlate well with accelerations derived from the stereo camera measured displacements shown in Figure 8. The discrepancy observed between the two sets of results are attributed to the distance between the optical tracking points and the locations of the accelerometers. The accelerometer data is considered valid for modal analysis purposes for the rest of the test campaign.

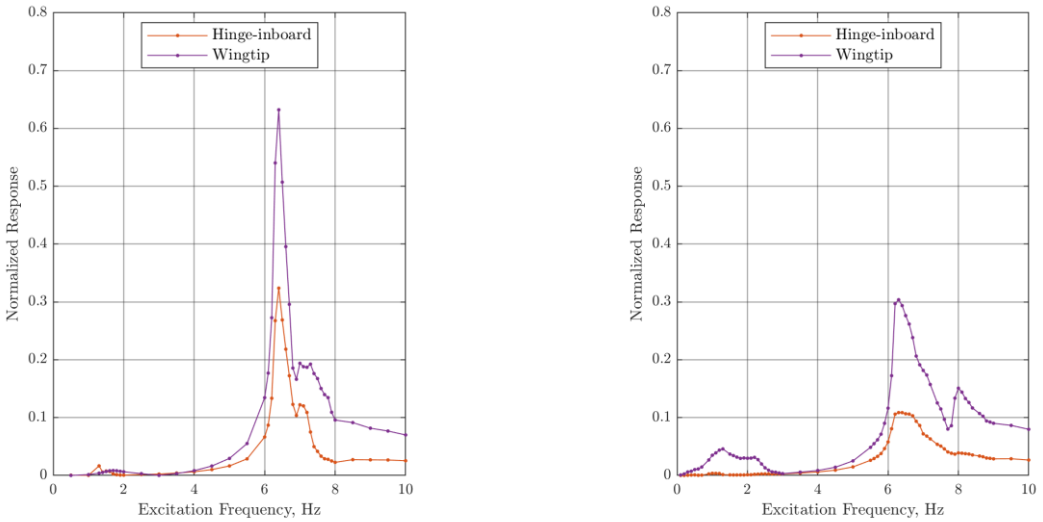

(a) The locked-hinge configuration. (b) The free-hinge configuration

Figure 9 In-plane acceleration due to gust excitation.

As shown in Figure 9, an in-plane bending mode exists within the tested frequency range at 6.4Hz in the locked-hinge configuration and at 6.3Hz in the free-hinge configuration. The wingtip response in the 1.0 to 2.0 Hz region is related to the folding degree of freedom.

B. Stepped-sine frequency sweep using wingtip tab

A series of stepped sine excitation up to 10.0Hz using the wingtip tab was conducted. The test condition was set to an angle of attack of 5.0 degrees and wind tunnel velocity of 18.0m/s, with sinusoidal wingtip tab actuation of +/- 10.0 degrees.

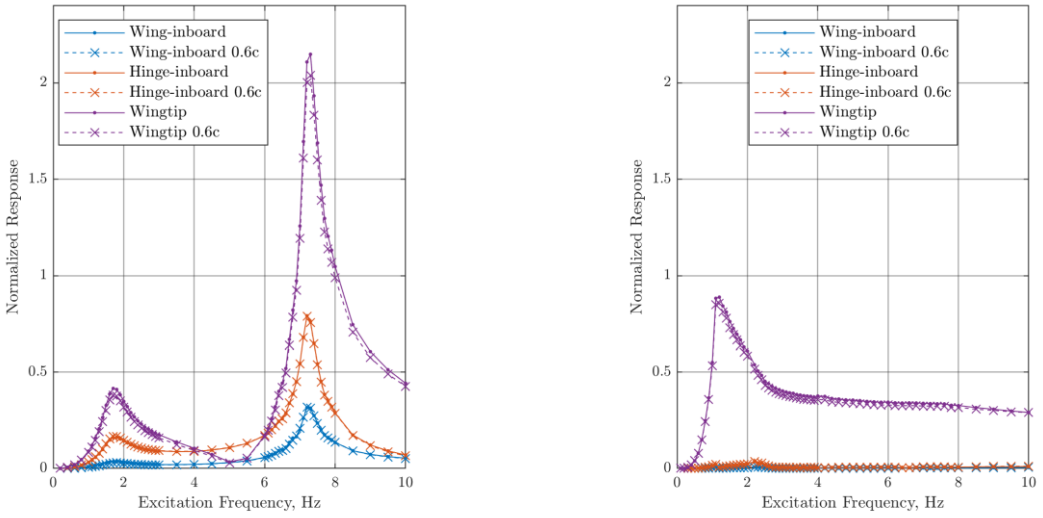

(a) The locked-hinge configuration. (b) The free-hinge configuration.

Figure 10 Out-of-plane acceleration due to wingtip tab excitation.

In the locked-hinge configuration, as shown in Figure 10(a), the change in aerodynamic forces due to the wingtip tab motion was able to excite the wing structure, producing a frequency response similar to the onset gust excitation

in Figure 7(a). However, with the wingtip in the free-hinge configuration, as shown in Figure 10(b), excitation from the tab input was limited to the wingtip itself due to the additional degree of freedom of the hinge. The frequency response of the wingtip motion peaks at 1.3Hz, which is a rigid body mode of the folding wingtip only.

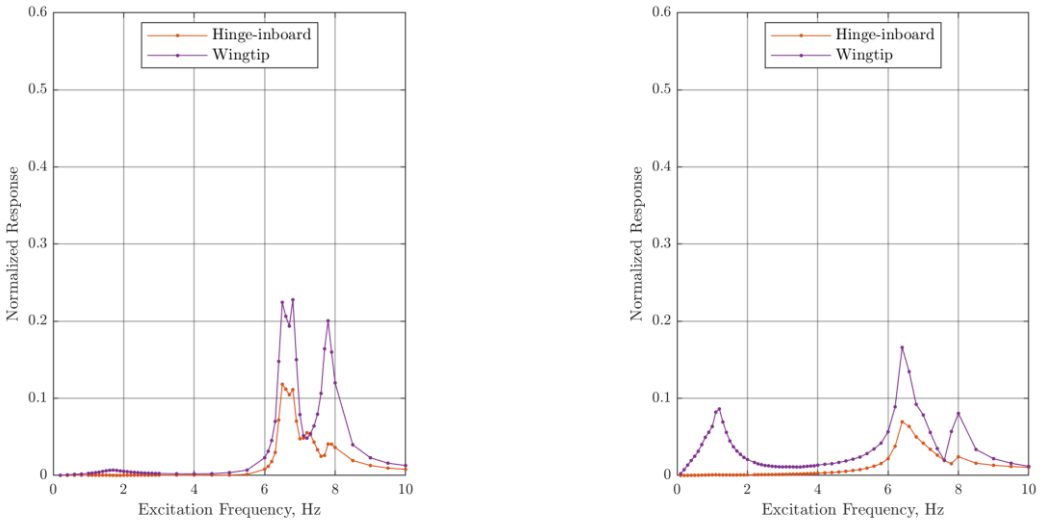

(a) The locked-hinge configuration. (b) The free-hinge configuration

Figure 11 In-plane acceleration due to wingtip tab excitation.

Figure 11(a) shows a similar frequency response in in-plane acceleration to the test cases in Figure 9(a), except for the peak at 7.8Hz, which was caused by the vibration of the onboard servo itself. In the free-hinge configuration, the in-plane acceleration response shown in Figure 11(b) also exhibits similarity to the onset gust excitation cases as seen in Figure 9(b), with the exception of the peak at 1.3Hz that coincides with the peak out-of-plane response. This is an expected observation due to the coupling inherited through the folding hinge geometry.

C. Pseudo-Random Gust

The pseudo-random gust sequence was used to generate a wider range of frequency excitation. This type of excitation has the advantage of consuming considerably less time when compared with the step-sine test, as well as representing the type of response experienced in-flight. The sequence was generated using the von Kármán power spectrum through a first order low-pass filter, with cut-off frequency set to 15.0Hz. The test condition was set to an angle of attack of 5.0 degrees and wind tunnel velocity of 18.0m/s.

Figure 12 and Figure 13 show the spectra of accelerometer measurements recorded during this gust excitation sequence. The Eigensystem realization algorithm (ERA)[17] was applied to the data correlations of these measurements to identify the modal frequencies and damping, which are shown in Table 2 and Table 3. The ERA solutions agree well with the modes found using the onset gust and wingtip tab frequency sweeps, revealing the attenuated response of the first mode in both hinge configurations were due to heavy damping. The extended frequency range of excitation in fact facilitated modal identification slightly beyond 15.0Hz, due to the gentle roll-off of the first order low-pass filter applied to the gust demand. The results obtained show the presence of an additional in-plane and out-of-plane bending mode for both hinge configurations in this extended frequency range.

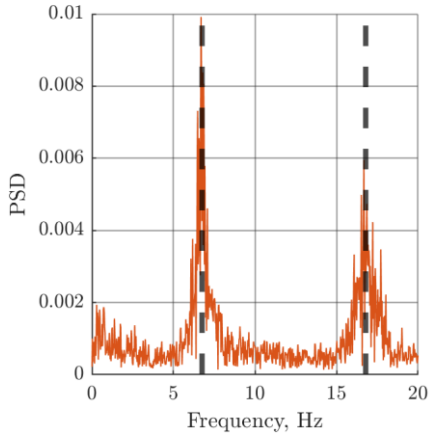

(a) In-plane acceleration inboard of the folding hinge

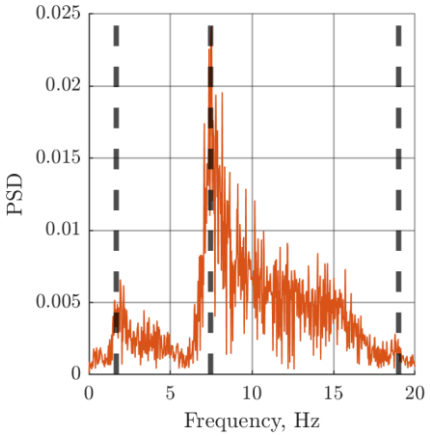

(b) Out-of-plane acceleration inboard of the folding hinge

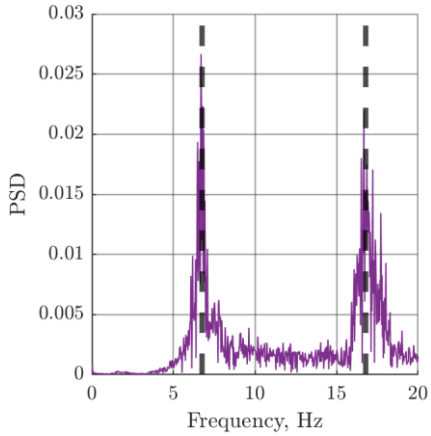

(c) In-plane acceleration at the wingtip

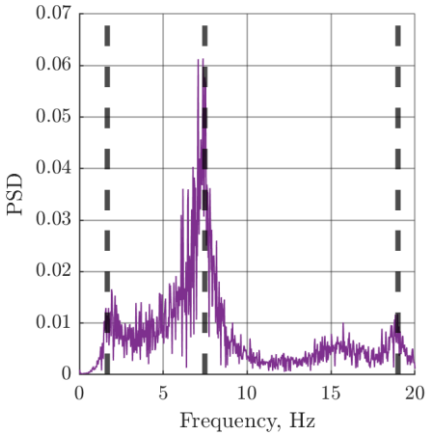

(d) Out-of-plane acceleration at the wingtip

Figure 12 Measured acceleration in the locked-hinge configuration during pseudo-random gust excitation. (Broken lines indicate ERA solutions)

Table 2. ERA solutions for the locked-hinge configuration.

Frequency, Hz	Damping Ratio, %	Modal Type
1.68	26.2	Out-of-plane bending
6.74	2.4	In-plane bending
7.47	4.7	Out-of-plane bending
16.79	1.9	In-plane bending
18.99	1.6	Out-of-plane bending

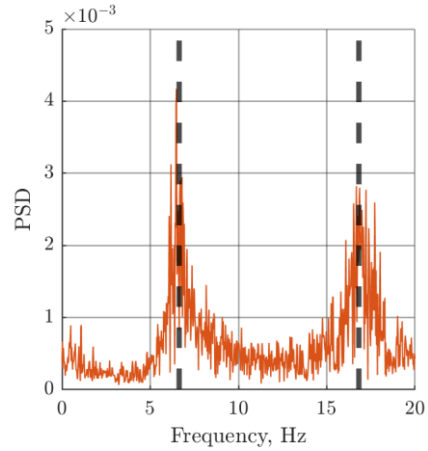

(a) In-plane acceleration inboard of the folding hinge

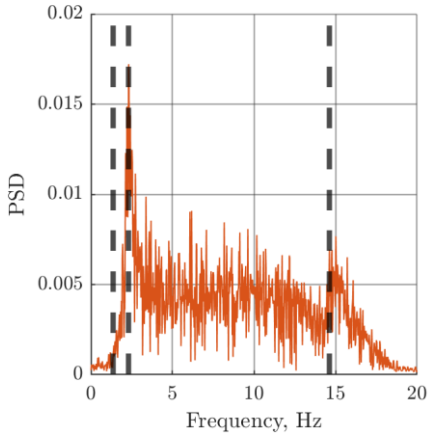

(b) Out-of-plane acceleration inboard of the folding hinge

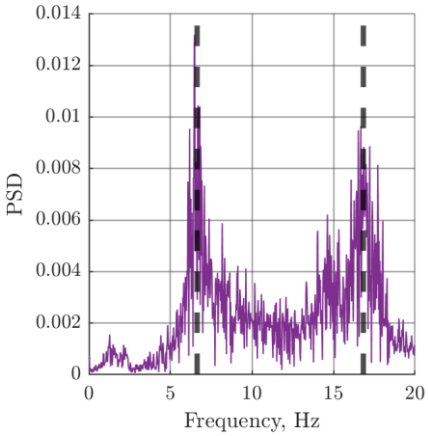

(c) In-plane acceleration at the wingtip

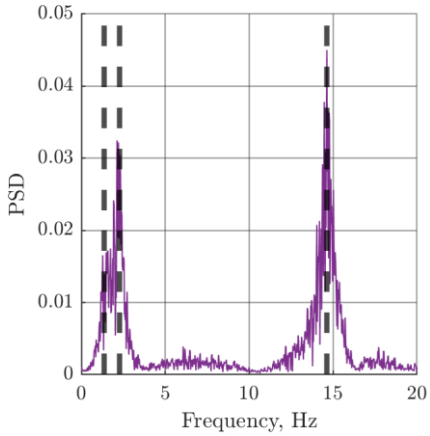

(d) Out-of-plane acceleration at the wingtip

Figure 13 Measured acceleration in the free-hinge configuration during pseudo-random gust excitation. (Broken lines indicate ERA solutions)

Table 3. ERA solutions for the free-hinge configuration.

Frequency, Hz	Damping Ratio, %	Modal Type
1.34	18.5	Out-of-plane bending, wingtip only
2.29	7.5	Out-of-plane bending
6.65	4.9	In-plane bending
14.63	1.5	Out-of-plane bending
16.83	2.9	In-plane bending

IV. Conclusions

The dynamic behavior of a flexible high aspect ratio wing fitted with a novel folding wingtip has been examined using non-contact excitations through aerodynamics. In wind-off condition, drooping of the folding wingtip would have posed significant difficulty for conventional modal testing. Therefore, the test methodology developed in this work aimed to allow the dynamic behavior to be measured with the folding wingtip aerodynamically trimmed at the wing-level orientation. The testing exploited the vertical gust generator fitted to the wind tunnel, as well as the tab onboard the folding wingtip itself as means of providing the excitation necessary for modal testing.

Sinusoidal frequency sweep using the gust generator and the wind-tip tab showed the basic modal frequencies could be established at the expense of long testing time. In the wingtip free-hinge configuration, the use of wingtip tab excitation was found to be crucial for determining the wingtip-only folding mode, as such mode could not be observed in the tests using the gust generator. However, the low transmissibility of high-frequency motion across the folding hinge limited the method's effectiveness at the high end of the frequency sweep.

The gust generator also had the capability in generating a pseudo-random gust sequence, which was used as a method of broadband excitation. The results from this gust sequence excitation showed excellent agreement with the previous frequency sweep tests, thus demonstrating the method's fitness as a faster testing method. Furthermore, through the eigensystem realization algorithm, damping ratios within the excitation frequency range were determined, of which the first mode was shown to be heavily damped.

References

[1]Lassen, M. A., Douglas, C. R., Jones, K. T., and Kenning, T. B., "Wing fold controller", U.S. Patent Application No. 14/022,622, Publication No. US20140014768A1,

[2]Cheung, R., Rezgui, D., Cooper, J., and Wilson, T. "Testing of a hinged wing-tip device for gust loads alleviation," *Journal of Aircraft* Vol. 55, No. 5, 2018, pp. 2050-2067.doi: 10.2514/1.C034811

[3]Castrichini, A., Siddaramaiah, V. H., Calderon, D. E., Cooper, J. E., Wilson, T., and Lemmens, Y. "Preliminary investigation of use of flexible folding wing tips for static and dynamic load alleviation," *The Aeronautical Journal* Vol. 121, No. 1235, 2017, pp. 73-94.doi: 10.1017/aer.2016.108

[4]Wilson, T., Castrichini, A., Azabal, A., Cooper, J. E., Ajaj, R., and Herring, M. "Aeroelastic Behaviour of Hinged Wing Tips," *International Forum on Aeroelasticity and Structural Dynamics*. Como, Italy, 2017.

[5]Cheung, R. C. M., Castrichini, A., Rezgui, D., Cooper, J. E., and Wilson, T. "Wind Tunnel Testing of Folding Wing-Tip Devices for Gust Loads Alleviation," *International Forum on Aeroelasticity and Structural Dynamics*. Como, Italy, 2017.

[6]Cheung, R. C., Rezgui, D., Cooper, J. E., and Wilson, T. "Testing of Folding Wing-Tip for Gust Load Alleviation in High Aspect Ratio Wing," *AIAA Scitech 2019 Forum*. 2019.

[7]Maxon, https://www.maxonmotor.co.uk/maxon/view/content/index, retrieved 2 December 2019

[8]RLS, https://www.rls.si/en/re22-rotary-magnetic-shaft-encoder, retrieved 2 december 2019

[9]Endevco, https://buy.endevco.com/65l-accelerometer.html, retrieved 2 december 2019

[10]PCB Piezotronics https://www.pcb.com/, retrieved 2 december 2019

[11]Vishay Micro-measurements, https://www.micro-measurements.com/, retrieved 2 december 2019

[12]AMTI, http://amti.uk.com/products/mc3a-6-axis-force-and-torque-sensor.php, retrieved 15 June 2017

[13]iMetrum, https://www.imetrum.com/, retrieved 2 december 2019

[14]National Instruments, http://www.ni.com/en-gb/shop/select/labview, retrieved 2 december 2019

[15]MATLAB, https://uk.mathworks.com/products/matlab.html, retrieved 2 december 2019

[16]Wood, K. T., Cheung, R. C., Richardson, T. S., Cooper, J. E., Darbyshire, O., and Warsop, C. "A New Gust Generator for a Low Speed Wind Tunnel: Design and Commissioning," *55th AIAA Aerospace Sciences Meeting*. American Institute of Aeronautics and Astronautics, 2017.

[17]Juang, J.-N. *Applied system identification*: Prentice-Hall, Inc., 1994.

Appendix

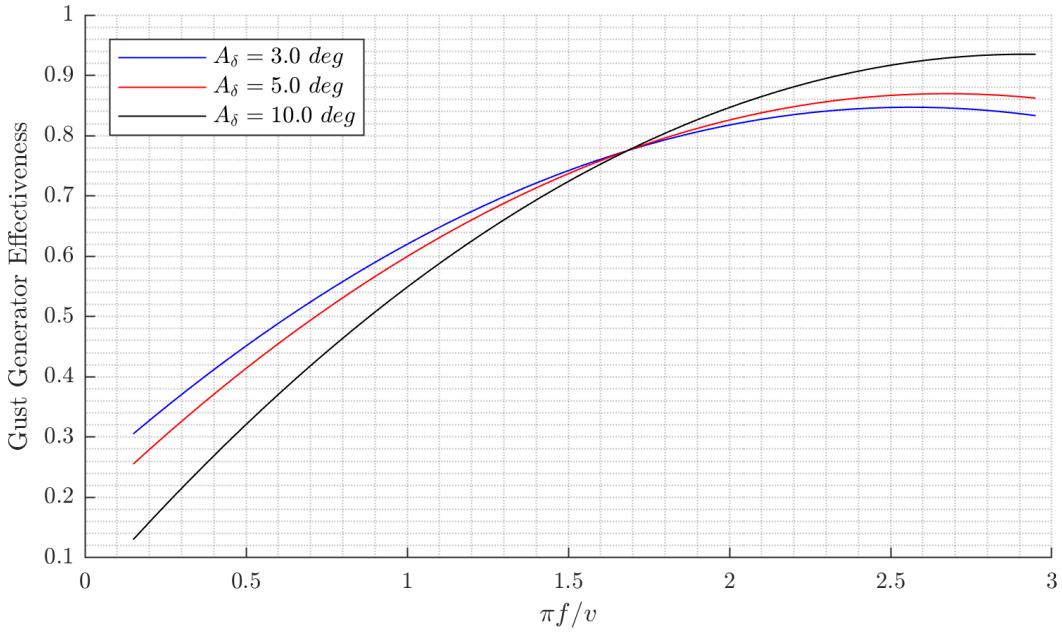

Figure A.1 Gust generator effectiveness.

The effectiveness of the gust generator when operating in the stepped-sine mode is defined as the ratio of the root-mean-square of the flow angle change caused by the gust generator, to the root-mean-square of the demand. The parameter, A_δ, denotes the peak demand angle.